Journal of Solid Mechanics Vol. 14, No. 1 (2022) pp. 99-117
DOI: 10.22034/jsm.2020.1903753.1618

Assessment of Different Mathematical Models for Analysis of Low-Velocity Impact on Composite Plates in Presence of Pre-loads

A. Davar *, A. Labbafian Mashhadi, J. Eskandari Jam, M. Heydari Beni

Faculty of Materials and Manufacturing Technologies, Malek Ashtar University of Technology, Tehran, Iran

Received 8 December 2021; accepted 16 January 2022

ABSTRACT

In this paper, the low-velocity impact response of composite plates in the presence of pre-loads is investigated using three new models for contact force estimation. The boundary conditions are considered as simply supported and the behavior of the material is linear elastic. The equations are based on both classical and first order shear deformation theory and the Fourier series method is used to solve the governing equations. The mass of the impactor is considered to be large mass and therefore the impact response is categorized as quasi-static. In the first impact model, the contact force history is first considered as a half-sine and then the maximum contact force and contact duration are calculated. In the second model, an improved two degree of freedom (ITDOF) spring-mass system is expressed by calculating the effective contact stiffness using a fast-iterative scheme. In the third model, which is expressed for the first time in this paper, the plate is considered as a series of masses and springs constructing a multi degree of freedom (MDOF) spring-mass system and the average forces applied to springs is introduced as the contact force. Validation of these models is done by comparing the results with the analytical, numerical and experimental results and shows good agreement. Results show that the new MDOF spring-mass system is more accurate for calculating the contact force rather than the ITDOF spring-mass system.

Keywords: Low-velocity impact; Composite plate; Impact force history; Quasi-static response.

1 INTRODUCTION

COMPOSITE laminates have received much attention in recent years and their applications in various industries, especially in the aerospace industries, are expanding day by day. Alongside this wide range of applications, most of these structures are exposed to external objects in their work environment. This impact can damage the composite structure and make it unusable. For example, dropping a tool on a composite piece while working can cause significant damage to its surface. However, this damage can sometimes occur internally and may

* Corresponding author. Tel.: +98 21 22945141.
E-mail address: a_davar@mut.ac.ir (A. Davar)

not be visible. Therefore, it is important to know the impact energy limit and, consequently, the maximum contact force on the impact that initiates the damage. In impact analysis, two parameters are of major concern. The first parameter is the estimation of the contact force and the second parameter is the prediction of displacements as well as strains in the target structure due to the impact. Many researchers have investigated the impact on composite plates. Some of these researchers have investigated the impact experimentally and studied the contact force, the displacement of the plate and the duration of the contact in the impact (Aslan et al. [4]; Karakuzu et al. [12]; Zouggar et al. [29]). Some of them have also analyzed the plate's response using numerical and finite element methods (Her and Liang [10]; Setoodeh et al. [21]; Ansari et al. [2]). Meanwhile, many researchers have tried to predict plate response using analytical methods. First time, Shivakumar et al. [22] applied analytical modeling of impact on composite structures. They presented two models. In the first model, using the energy balance between the impact kinetic energy and the sum of the energies spent on the deformation of the structure, they were able to calculate the contact force. In the second model, the impactor and plate were considered as two rigid masses and their deformation as two springs. Then, by applying an initial velocity to the impactor and obtaining the response of the system, they obtained a time history of the contact force and the plate's displacement. Pierson and Vaziri [20] using the first-order shear deformation theory, proposed a model for analyzing the behavior of special orthotropic plates with simply supported conditions. Their model was based on the Hertz nonlinear contact law. Olsson [17] classified the low-velocity impact according to the impactor mass to target structure mass ratio into two categories of small mass and large mass. When the impactor mass is larger than the mass of the target structure, the structure exhibits a quasi-static behavior. Abrate [1] has studied extensively the behavior of impacted composite structures. His models include spring-mass models, energy balance models, complete models and a model for analysis of impact on infinite plates. Christoforou [7] provided a reverse response for the low-velocity impact of composite plates. They were able calculate the mass and velocity of the impactor with experimental dynamic response. Choi and Lim [5] investigated the low-velocity impact on composite laminates using the Hertz linear contact law. Khalili et al. [14] investigated the effect of initial stresses on transverse impact response of composite plates. Payeganeh et al. [19] analyzed the dynamic response of FML laminates under low-velocity impact using a two degree of freedom spring-mass system and using the Hertz linearized contact model presented by Choi. Khalili et al. [13] investigated the transverse impact response on FGM composite plates considering the effect of temperature on the properties. Feli et al. [9] presented a new analytical model for behavior of CNT reinforced composite plates under low-velocity impact. Huo et al. [11] studied low-velocity impact response of foam-core sandwich panels analytically and experimentally. Patil and Reddy [18] studied oblique low-velocity impact on composite plate numerically.

In this paper, three models for low-velocity impact on composite plates in the presence of pre-loads are presented. The basis of the first model is the estimation of the contact force as a function of half-sine. In the second model, the impactor and plate are considered as a two degree of freedom spring-mass system and the stiffness of the contact is determined using iterative cycle. In the third model, the stiffness of the plate is considered as a series of springs and by the Fourier series method, the stiffness of each spring is determined. Also, the mass of the participant in each mode is calculated after calculating the natural frequency of the plate in that mode. Finally, the average of forces applied to the springs is referred to as the contact force.

2 GOVERNING EQUATIONS

A composite laminate with length a, width b and thickness h is shown in Fig. 1. The center of the xyz orthogonal coordinate system is located in the mid-plane of this laminate. The displacement components along the x, y and z directions are defined by u, v and w respectively. In this section, the equations for static deflection, critical buckling load and natural frequency of plate are examined for both classical and first-order shear deformation theories.

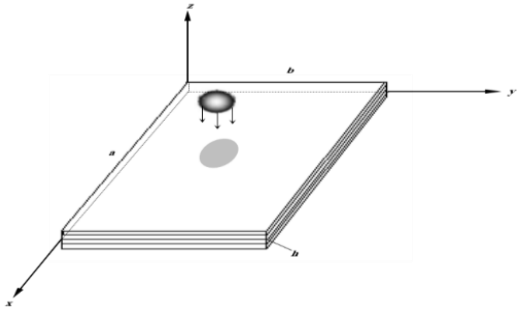

Fig.1
Schematic of a composite plate under central impact.

2.1 Classical plate theory (CPT)

In the classical plate theory, the effects of shear deformation and rotational inertia are ignored. So, the assumed displacement field is given by (Whitney [28]):

$$\begin{aligned} u &= u^0(x,y,t) - z w_{,x}(x,y,t) \\ v &= v^0(x,y,t) - z w_{,y}(x,y,t) \\ w &= w(x,y,t) \end{aligned} \tag{1}$$

where u^0, v^0, and w are the plate displacements in the x, y, and z directions at the plate's mid-plane and the differentiation respect to x or y is denoted by a comma. The equations of motions of an especially orthotropic plate with considering uniform initial stress resultants N_x and N_y and applied force p_z are (Whitney [28]):

$$D_{11}w_{,xxxx} + 2(D_{12} + 2D_{66})w_{,xxyy} + D_{22}w_{,yyyy} + \rho_0 \ddot{w} = p_z + N_x w_{,xx} + N_y w_{,yy} \tag{2}$$

where ρ_0 is the plate mass per unit area and differentiation with respect to time is denoted by a dot. Also, the values for the flexural stiffness of the plate are (Whitney [28]):

$$D_{ij} = \int_{-h2}^{h/2} z^2 \overline{Q}_{ij}\, dz \qquad (i,j = 1,2,6) \tag{3}$$

where $\overline{Q}_{ij}$ is the reduced stiffness matrix. For a simply supported plate the following boundary conditions are applicable (Whitney [28]):

$$\begin{aligned} w &= 0 \quad \text{at } x = 0, a \\ w &= 0 \quad \text{at } y = 0, b \end{aligned} \tag{4}$$

2.1.1 Static loading

For a static load, solution to Eq. (2) that satisfy the boundary conditions Eq. (4) are given by (Ugural [25]):

$$W = A_{mn} \sin(m\pi x/a)\sin(n\pi y/b) \tag{5}$$

and the loading function given by (Ugural [25]):

$$p_z = q_{mn} \sin(m\pi x/a)\sin(n\pi y/b) \tag{6}$$

where q_{mn} is the term of a Fourier series representation of the load. For a concentrated force p which is applied at a point to the (x_1, y_1) of the plate, q_{mn} are given by (Ugural [25]):

$$q_{mn} = \frac{4p}{ab} \sin(m\pi x_1/a)\sin(n\pi y_1/b) \tag{7}$$

Substituting Eqs. (5) and (6) into the equation of motion Eq. (2) produces:

$$A_{mn} = \frac{a^4 q_{mn}}{\pi^4 \left[D_{11}m^4 + 2\left(D_{12} + 2D_{66}\right)\left(mnR\right)^2 + D_{22}\left(nR\right)^4 + N_x\left(\frac{ma}{\pi}\right)^2 + N_y\left(\frac{nRa}{\pi}\right)^2 \right]} \tag{8}$$

where $R = a/b$ is the aspect ratio of the plate. The displacement at any point in the plate may be calculated as (Ugural [25]):

$$w = \sum_{m=1}^{M}\sum_{n=1}^{N} A_{mn} \sin(m\pi x/a)\sin(n\pi y/b) \tag{9}$$

where m and n are the half-wave counters and M and N are the half-wave numbers in the x and y respectively.

2.1.2 Critical buckling load

In order to find the critical value of the loads N_x and N_y we must utilize Eq. (2) with initial in-plane force effects and $p_z = 0$. Considering a form similar to Eq. (5) for the deflection and Substituting it into Eq. (2) produces (Whitney [28]):

$$\pi^2\left[D_{11}m^4 + 2(D_{12}+2D_{66})m^2n^2R^2 + D_{22}n^4R^4\right] = -a^2\left[N_X m^2 + N_y n^2R^2\right] \tag{10}$$

The in-plane loads considered of the form (Whitney [28]):

$$N_x = -N_0 N_y = -kN_0 \tag{11}$$

where $N_0>0$ and k denote the ratio of N_y/N_x. Therefore from Eq. (10) obtained (Whitney [28]):

$$N_0 = \frac{\pi^2\left[D_{11}m^4 + 2(D_{12}+2D_{66})m^2n^2R^2 + D_{22}n^4R^4\right]}{a^2(m^2 + kn^2R^2)} \tag{12}$$

The critical buckling load corresponds to the value of m and n which yields the lowest value of N_0.

2.1.3 Natural frequency

The governing equation for free vibration can be obtained from Eq. (2) by ignoring the lateral load (p_z). The solution to this equation must satisfy the boundary condition as well as the initial conditions with respect to time. The solution considered of the form (Whitney [28]):

$$w = A_{mn} \sin(m\pi x/a)\sin(n\pi y/b)e^{i\omega t} \tag{13}$$

where ω is the natural frequency of vibration. Substituting Eq. (13) into the governing equation and solving the natural frequency obtained:

$$\omega_{mn}^2 = \frac{\pi^4}{\rho_0 a^4}\left(D_{11}m^4 + 2\left(D_{12}+2D_{66}\right)m^2n^2R^2 + D_{22}n^4R^4 + N_x\left(\frac{ma}{\pi}\right)^2 + N_y\left(\frac{nRa}{\pi}\right)^2\right) \tag{14}$$

2.2 First order shear deformation theory (FSDT)

In the first order shear deformation theory the assumed displacement field is given by (Dobyns [8]):

$$\begin{aligned} u &= u^0(x,y,t) + z\psi_x(x,y,t) \\ v &= v^0(x,y,t) + z\psi_y(x,y,t) \\ w &= w(x,y,t) \end{aligned} \tag{15}$$

where ψ_x and ψ_y are the shear rotations in the x and y directions. The equations of motion of a special orthotropic plate with considering uniform initial stress resultants are (Dobyns [8]):

$$\begin{aligned}
&D_{11}\psi_{x,xx}+D_{66}\psi_{x,yy}+\left(D_{12}+D_{66}\right)\psi_{y,xy}-\kappa A_{55}\psi_x-\kappa A_{55}w_{,x}=I\ddot{\psi}_x\\
&\left(D_{12}+D_{66}\right)\psi_{x,xy}+D_{66}\psi_{y,xx}+D_{22}\psi_{y,yy}-\kappa A_{44}\psi_y-\kappa A_{44}w_{,y}=I\ddot{\psi}_y\\
&\kappa A_{55}\psi_{x,x}+\left(\kappa A_{55}+N_x\right)w_{,xx}+\kappa A_{44}\psi_{y,y}+\left(\kappa A_{44}+N_y\right)w_{,yy}+p_z=P\ddot{w}
\end{aligned} \tag{16}$$

where κ is a shear correction factor and is popularly taken to be $\pi^2/12$ and the inertias are given by (Dobyns [8]):

$$\begin{aligned}
&A_{ij}=\int_{-h/2}^{h/2}\bar{Q}_{ij}dz \qquad ij=1,2,6\\
&A_{ij}=\int_{-h/2}^{h/2}C_{ij}dz \quad i,j=4,5\\
&\left(P,I\right)=\int_{-h/2}^{h/2}\rho\left(1,z^2\right)dz
\end{aligned} \tag{17}$$

where ρ is density of plate and C_{ij} are transverse shear stiffnesses, as defined by (Whitney and Pagano [27]). For a simply supported rectangular plate of uniform thickness the boundary conditions are given by (Dobyns [8]):

$$\begin{aligned}
&w=\psi_{x,x}=0 \text{ at } x=0,a\\
&w=\psi_{y,y}=0 \text{ at } y=0,b
\end{aligned} \tag{18}$$

2.2.1 Static loading

For a static load, solutions to Eq. (16) that satisfy the boundary conditions Eq. (18) are given by (Dobyns [8]):

$$\begin{aligned}
&\Psi_x=A_{mn}\cos\left(m\pi x/a\right)\sin\left(n\pi y/b\right)\\
&\Psi_y=B_{mn}\sin\left(m\pi x/a\right)\cos\left(n\pi y/b\right)\\
&W=C_{mn}\sin\left(m\pi x/a\right)\sin\left(n\pi y/b\right)
\end{aligned} \tag{19}$$

and the loading function is given by an equation similar to Eq. (6). Substituting Eq. (19) and the loading function into the equations of motion Eq. (16) produces (Dobyns [8]):

$$\begin{bmatrix}L_{11} & L_{12} & L_{13}\\ L_{12} & L_{22} & L_{23}\\ L_{13} & L_{23} & L_{33}\end{bmatrix}\begin{Bmatrix}A_{mn}\\ B_{mn}\\ C_{mn}\end{Bmatrix}=\begin{Bmatrix}0\\ 0\\ q_{mn}\end{Bmatrix} \tag{20}$$

where the values for the matrix parameters are given in Dobyns [8]. By solving Eq. (20) for C_{mn} the displacement at any point in the plate may be calculated as (Dobyns [8]):

$$w=\sum_{m=1}^{M}\sum_{n=1}^{N}C_{mn}\sin\left(m\pi x/a\right)\sin\left(n\pi y/b\right) \tag{21}$$

2.2.2 Critical buckling load

Considering a form similar to Eq. (19) and Substituting it into Eq. (16) without the term including time and transverse load produces:

$$\begin{bmatrix} L_{11} & L_{12} & L_{13} \\ L_{12} & L_{22} & L_{23} \\ L_{13} & L_{23} & L_{33} \end{bmatrix} \begin{Bmatrix} A_{mn} \\ B_{mn} \\ C_{mn} \end{Bmatrix} = \begin{Bmatrix} 0 \\ 0 \\ 0 \end{Bmatrix} \tag{22}$$

By setting determinant of the coefficients equal to zero, the buckling load is calculated. Moh and Hwu [16] found an equation to calculate the critical buckling load (Vinson and Sierakowski [26]):

$$\begin{aligned}
N_0 &= \frac{(1+\eta)p_0}{\left[1+k\,(an/bm)^2\right](1+\eta_x+\eta_y+\eta_0)} \\
\eta &= \pi^2 D^* \left[\frac{1}{A_{44}}\left(\frac{m}{a}\right)^2 + \frac{1}{A_{55}}\left(\frac{n}{b}\right)^2 \right] \\
\eta_x &= \frac{\pi^2}{A_{55}}\left[D_{11}\left(\frac{m}{a}\right)^2 + D_{66}\left(\frac{n}{b}\right)^2 \right] \\
\eta_y &= \frac{\pi^2}{A_{44}}\left[D_{66}(\frac{m}{a})^2 + D_{22}(\frac{n}{b})^2 \right] \\
\eta_0 &= \frac{D^* p_0 m^2 n^2}{a^2 A_{55} A_{44}} \\
p_0 &= \frac{\pi^2 a^2}{m^2}\left[D_{11}\left(\frac{m}{a}\right)^4 + 2\left(D_{12}+2D_{66}\right)\left(\frac{m}{a}\right)^2\left(\frac{n}{b}\right)^2 + D_{22}\left(\frac{n}{b}\right)^4 \right] \\
D^* p_0 &= \frac{\pi^2 a^2}{m^2}\left\{ D_{11}D_{66}\left(\frac{m}{a}\right)^4 + \left[D_{12}D_{22} - D_{12}\left(D_{12}+2D_{66}\right)\right]\left(\frac{m}{a}\right)^2\left(\frac{n}{b}\right)^2 + D_{22}D_{66}\left(\frac{n}{b}\right)^4 \right\}
\end{aligned} \tag{23}$$

The critical buckling load corresponds to the value of m and n which yields the lowest value of N_0.

2.2.3 Natural frequency

The frequency of natural vibration may be computed by assuming for displacements (Dobyns [8]):

$$\psi_x = \Psi_x e^{i\omega t} \qquad \psi_y = \Psi_y e^{i\omega t} \qquad w = W e^{i\omega t} \tag{24}$$

where Ψ_x , Ψ_y , and W are given by Eq. (19). Substituting the assumed displacements Eq. (24) into the equations of motion Eq. (16) results in (Dobyns [8]):

$$\begin{aligned}
&D_{11}\Psi_{x,xx_{mn}} + D_{66}\Psi_{x,yy_{mn}} + (D_{12}+D_{66})\Psi_{y,xy_{mn}} - \kappa A_{55}\Psi_{x_{mn}} - \kappa A_{55}W_{,x_{mn}} = -\omega_{mn}^2 I \Psi_{x_{mn}} \\
&(D_{12}+D_{66})\Psi_{x,xy_{mn}} + D_{66}\Psi_{y,xx_{mn}} + D_{22}\Psi_{y,yy_{mn}} - \kappa A_{44}\Psi_{y_{mn}} - \kappa A_{44}W_{,y_{mn}} = -\omega_{mn}^2 I \Psi_{y_{mn}} \\
&\kappa A_{55}\Psi_{x,x_{mn}} + (\kappa A_{55} + N_x^0)W_{,xx_{mn}} + \kappa A_{44}\Psi_{y,y_{mn}} + (\kappa A_{44} + N_y^0)W_{,yy_{mn}} = -\omega_{mn}^2 P W_{mn}
\end{aligned} \tag{25}$$

Substituting Eq. (19) and its derivatives into Eq. (25) results in a set of homogeneous equations that may be solved for the natural frequencies of vibration (Dobyns [8]):

$$\begin{bmatrix} L'_{11} & L_{12} & L_{13} \\ L_{12} & L'_{22} & L_{23} \\ L_{13} & L_{23} & L'_{33} \end{bmatrix} \begin{Bmatrix} A'_{mn} \\ B'_{mn} \\ C'_{mn} \end{Bmatrix} = \begin{Bmatrix} 0 \\ 0 \\ 0 \end{Bmatrix} \tag{26}$$

where L'_{11}, L'_{22}, and L'_{33} are given by (Dobyns [8]):

$$L'_{11} = L_{11} - \omega_{mn}^2 I \qquad L'_{22} = L_{22} - \omega_{mn}^2 I \qquad L'_{33} = L_{33} - \omega_{mn}^2 P \tag{27}$$

Three eigenvalues and their respective eigenvectors result from Eq. (26) for each *m*, *n* pair and natural frequencies and mode shapes are obtained.

3 NEW CONTACT FORCE ESTIMATION PROCEDURES

First, to prepare the initial information, the static displacement of the plate under concentrated unit force (p = 1) at the point (x_1, y_1) is calculated from Eq. (9) or Eq. (21) and then the global static stiffness (K_{bs}) is obtained from:

$$K_{bs} = \frac{p}{w(x_1, y_1)} \tag{28}$$

Also, the natural frequency of the plate in different modes is calculated for both CLT and FSDT and the smallest (fundamental frequency ω_f) is determined. Based on this preliminary data, three new models for estimating the contact force are introduced: the half-sine (HS) model, the improved two degree of freedom (ITDOF) model, and the multi degree of freedom (MDOF) model. In all of these models, the impactor mass (isotropic sphere) relative to plate mass is assumed to be large and thus the impact response is assumed to be quasi-static.

3.1 Half-Sine model (HS)

Because the impactor mass is large relative to the mass of the plate, the nature of the plate response is quasi-static, and therefore this response can be considered as a half-sine function (Olsson [17]). The maximum contact force (F_{max}) is calculated using energy balance method from (Apetre et al. [3]):

$$\frac{F_{\max}^2}{2K_{bs}} = \frac{F_{\max}^{1+1/\mu}}{(\mu+1)K^{1/\mu}} = \frac{1}{2} M_i V_0^{\,2} \tag{29}$$

where M_i and V_0 are mass and initial velocity of the impactor. According to Hertz contact law, μ is assumed to be 1.5. Also, K is the Hertz contact stiffness obtained from (Abrate [1]):

$$K = \frac{4}{3} E_{eff} R_{eff}^{1/2} \qquad \frac{1}{R_{eff}} = \frac{1}{R_1} + \frac{1}{R_2} \qquad \frac{1}{E_{eff}} = \frac{1-\nu_1^2}{E_1} + \frac{1-\nu_2^2}{E_2} \tag{30}$$

In this Equations subtitle 1 is related to the impactor and subtitle 2 is related to the target structure. Since in this paper a flat plate is considered, so R_2 is infinite and R_{eff} is equal to the radius of impactor. The characteristic equation of the system of a plate with length a, width b and mass M_p with a point mass M_i attached at the plate in impact point (x_1, y_1) on the mid-plane of the plate is (Soedel [23]):

$$\frac{4}{M_p} \sum_{m=1}^{M} \sum_{n=1}^{N} \frac{1}{(\omega_{mn}^2 - \omega_k^2)} \sin^2\left(\frac{m\pi x_1}{a}\right) \sin^2\left(\frac{n\pi y_1}{b}\right) - \frac{1}{M_i \omega_k^2} = 0 \tag{31}$$

where ω_k is the natural frequency of the system consists of the plate and the mass attached to it. After solving this equation, the lowest value of the ω_k will be the fundamental frequency of the system (ω_1^*). Finally, the contact force $F_c(t)$ is obtained by estimating a half-sine function according to the following equation:

$$F_c(t) = F_{\max} \sin(\omega_1^* t), \qquad 0 \le t \le \pi / \omega_1^* \tag{32}$$

Flowchart of the present HS contact force estimation procedure is indicated in Fig. 2.

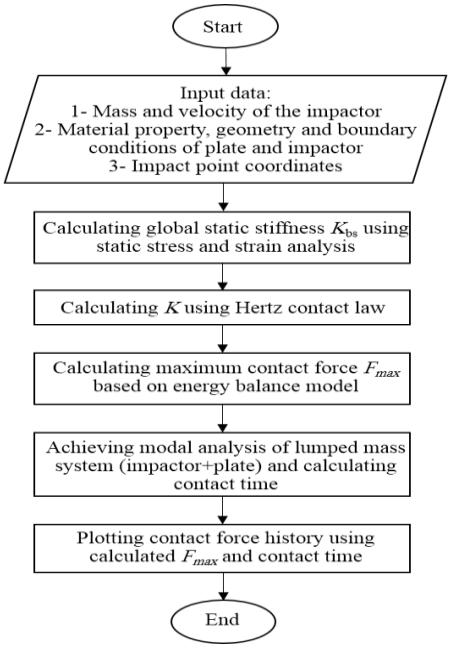

Fig.2
Flowchart of the present HS model.

3.2 Improved two degree of freedom spring-mass model (ITDOF)

In this model, the impactor and plate are expressed as two rigid bodies and their deformation as two springs. The initial impact velocity is V_0 and the other initial conditions are considered zero. Schematic of this model shown in Fig. 3.

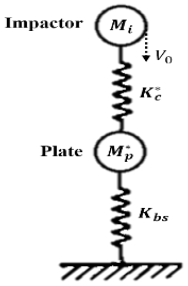

Fig.3
Schematic of the two degree of freedom impact model.

According to Newton's second law, the equation of motion of this two degree of freedom system is:

$$\begin{bmatrix} M_i & 0 \\ 0 & M_p^* \end{bmatrix} \begin{Bmatrix} \ddot{x}_i \\ \ddot{x}_p \end{Bmatrix} + \begin{bmatrix} K_c^* & -K_c^* \\ -K_c^* & (K_c^* + K_{bs}) \end{bmatrix} \begin{Bmatrix} x_i \\ x_p \end{Bmatrix} = \begin{Bmatrix} 0 \\ 0 \end{Bmatrix} \tag{33}$$

where M_i and M_p^* are the impactor mass and effective plate mass, K_c^* and K_{bs} are the effective (modified) contact stiffness and the global bending stiffness of the plate, and x_i and x_p are the impactor and plate displacements, respectively. Swanson presented an approximate relation for effective mass estimation (Swanson [24]):

$$\omega_f \approx \sqrt{\frac{K_{bs}}{M_p^*}} \tag{34}$$

where ω_f is the lowest natural frequency of the plate. The calculated effective mass from this equation is used in the present model. The contact force $F_c(t)$ is obtained by solving Eq. (33):

$$F_c(t) = K_{bs} x_p(t) = \frac{K_{bs} V_0 (K_c^* - M_i \omega_2^2)(K_c^* - M_i \omega_1^2)}{K_c^* M_i (\omega_1^2 - \omega_2^2)} \times \left(\frac{\sin(\omega_1 t)}{\omega_1} - \frac{\sin(\omega_2 t)}{\omega_2} \right) \tag{35}$$

where ω_1 and ω_2 are the natural frequencies of the two degree of freedom spring-mass system. The effective contact stiffness used in Eq. (35) is obtained from an iterative scheme. In the first iteration, the maximum contact force is obtained from (Choi and Lim [5]):

$$F_m^{(1)} = V_0 \sqrt{K_{bs} M_i} \tag{36}$$

Then the effective contact stiffness is calculated from (Choi and Lim [5]):

$$K_c = F_m^{1/3} K^{2/3} \tag{37}$$

where K is the Hertz contact stiffness. Using this effective stiffness, the maximum contact force can be achieved again. This action will be repeated until the maximum contact force does not change. The rate of convergence is very fast. Finally, the correct effective contact stiffness (K_c^*) will be calculated and by replacing it in Eq. (35) contact force history will be obtained. Flowchart of the present ITDOF model shown in Fig. 4.

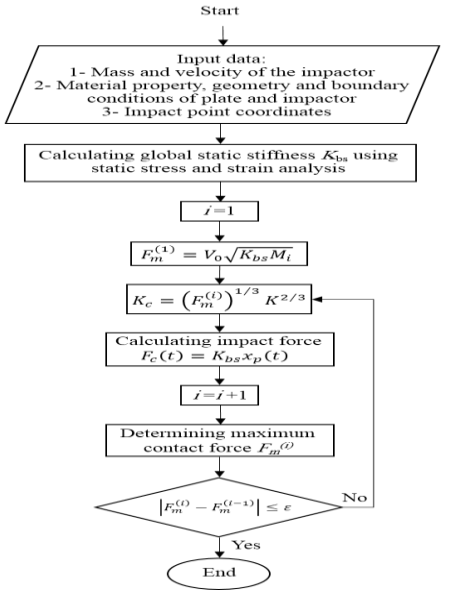

Fig.4
Flowchart of the present ITDOF model.

3.3 Multi degree of freedom spring-mass model (MDOF)

In this model, instead of considering a spring equivalent to the global stiffness of the plate, the plate is considered as a system consisting of $M \times N$ mass and series springs, according to Fig. 5. For this purpose, the plate considered as an equivalent lamina and according to the superposition principle, the contribution of each mode (m, n) of the plate can be defined as a single spring and mass. If the unit load that is quasi-static applied at (x_1,y_1) in the plate, each spring has the same force share, but the displacement at this point arising from each mode (m, n) is proportional to the deformation of each individual spring and the rate of this deformation also depends on the stiffness of the spring.

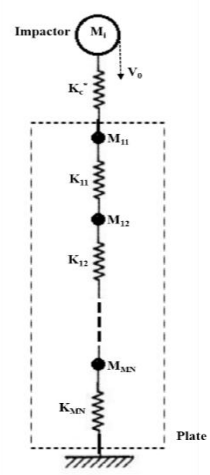

Fig.5
Schematic of the multi degree of freedom impact model.

Firstly, using Eq. (5) or Eq. (19) the displacement of plate in each mode (m, n) shown with w_{mn} and calculated. Then, considering concentrated unit force (p = 1) the stiffness of each spring corresponding to each mode (m, n) in the static deformation shown with K_{mn} and obtained from:

$$K_{mn} = \frac{p}{w_{mn}} \tag{38}$$

The natural frequency of the bending vibrations of the plate at each mode (ω_{mn}) calculated and then the contribution of the participant's mass to the vibration of the plate in each mode at the point of impact shown with M_{mn} and obtained from:

$$M_{mn} = \frac{K_{mn}}{\omega_{mn}^2} \tag{39}$$

In this model, the effective contact stiffness is obtained in a process similar to the ITDOF model. After determining the mass and stiffness values of each mode, with considering the effective contact stiffness as the first spring, the equation of motion of this (M×N) +1 degree of freedom system is:

$$\begin{bmatrix} M_i & 0 & 0 & 0 & 0 & 0 \\ 0 & M_{11} & 0 & 0 & 0 & 0 \\ 0 & 0 & M_{12} & 0 & 0 & 0 \\ 0 & 0 & 0 & M_{13} & 0 & 0 \\ 0 & 0 & 0 & 0 & \ddots & 0 \\ 0 & 0 & 0 & 0 & 0 & M_{MN} \end{bmatrix} \begin{Bmatrix} \ddot{x}_i \\ \ddot{x}_{11} \\ \ddot{x}_{12} \\ \ddot{x}_{13} \\ \vdots \\ \ddot{x}_{MN} \end{Bmatrix} + \begin{bmatrix} K_c^* & -K_c^* & 0 & 0 & 0 & 0 \\ -K_c^* & K_c^*+K_{11} & -K_{11} & 0 & 0 & 0 \\ 0 & -K_{11} & K_{11}+K_{12} & 0 & 0 & 0 \\ 0 & 0 & 0 & \ddots & 0 & 0 \\ 0 & 0 & 0 & 0 & K_{M(N-2)}+K_{M(N-1)} & -K_{M(N-1)} \\ 0 & 0 & 0 & 0 & -K_{M(N-1)} & K_{M(N-1)}+K_{MN} \end{bmatrix} \begin{Bmatrix} x_i \\ x_{11} \\ x_{12} \\ x_{13} \\ \vdots \\ x_{MN} \end{Bmatrix} = \begin{Bmatrix} 0 \\ 0 \\ 0 \\ 0 \\ \vdots \\ 0 \end{Bmatrix} \tag{40}$$

where x_i is displacement of impactor and x_{mn} is displacement of any of the M_{mn} masses. By solving this equation, the average of the forces applied to the springs is the contact force and obtained from:

$$F_c(t) = \frac{1}{M \times N} \sum_{m=1}^{M} \sum_{n=1}^{N} F_{mn} \tag{41}$$

By applying the unit central load on the plate, the stiffness of the springs in the MDOF model for M=N=20 in a specific case is calculated from Eq. (38) and shown in Fig. 6. When the impact is applied to the center of the plate (concentrated static load), the contributory mass for all modes is equal to one-fourth the mass of the plate, and the displacement of the plate is only calculated for the odd modes. As expected, as the number of modes increases, the

plate displacement under a constant static load decreases in each mode and therefore the stiffness corresponding each mode increases. The final value of *M* and *N* for use in this model is the number of modes in which the plate deflection to convergence. Also, because the impactor only contacts the first mass in the set of masses, the displacement of the first mass is considered as the displacement of the plate during impact. Flowchart of the present MDOF model shown in Fig. 7.

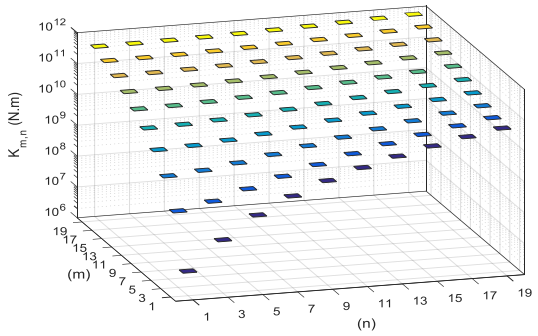

Fig.6
Stiffness of springs in different modes.

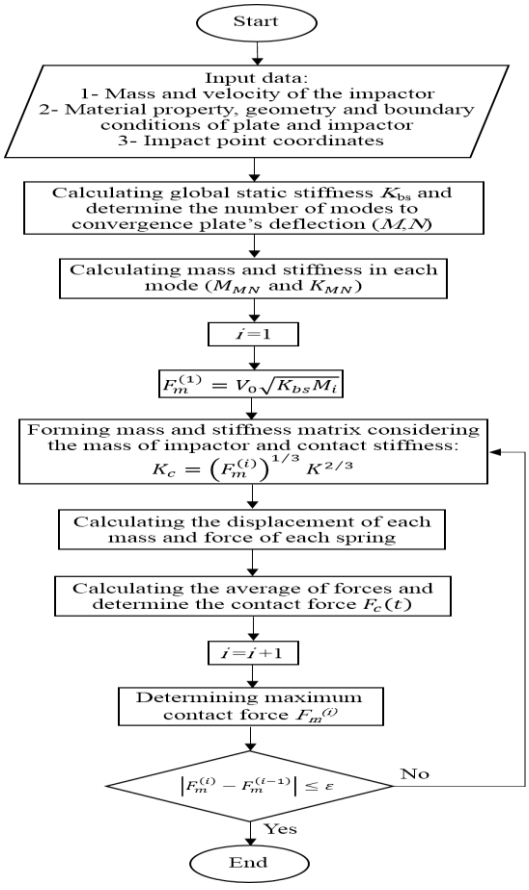

Fig.7
Flowchart of the present MDOF model.

4 NUMERICAL SIMULATIONS

In order to validate the models presented in this paper, in addition to the available references, numerical results from the ABAQUS software have also been used. For this purpose, the analysis was performed with ABAQUS/Explicit solver. The Analytical Rigid type used for impactor modeling. For composite plate layering, Conventional Shell elements and in plate meshing, S4R elements are used. The arrangement of the meshes modeled from Khalili et

al.[15] according to Fig. 8. Plate elements are Quad type and the Free technique is applied to mesh. Penalty Contact is used to simulate the contact between the impactor and the plate. Vertical contact behavior is defined as Hard Contact and tangential contact behavior is defined as Frictionless. The boundary conditions of the plate are simply supported and the impactor can only be moved in the impact direction. The initial velocity of the impactor is assigned to a reference point on the imoactor using Predefined Field and the initial loads applied as the shell edge load. Also, since the purpose of this article is to investigate the low-velocity impact and find the contact force before reaching to damage, very minor damage at the impact site is ignored and the simulation does not enter to damage range in the plate. The area of impact after the impact in a specific case is shown in Fig. 9.

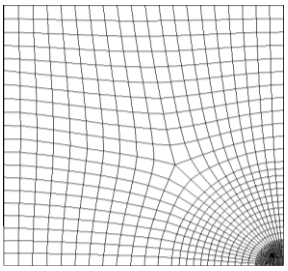

Fig.8
Mesh pattern of the plate (Khalili et al. [15]).

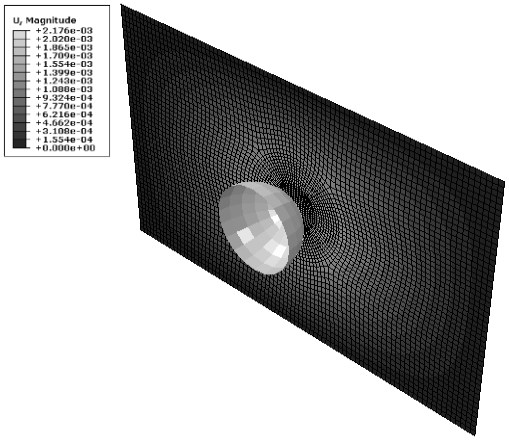

Fig.9
Relative position of impactor and plate and plate's deflection contour after impact.

5 RESULTS AND DISCUSSION

In order to validate the presented models, first the results without considering pre-loads are compared with Pierson and Vaziri [20] analytical model Delfosse. Experimental results which are adapted from Pierson and Vaziri [20]. Then the results with considering pre-loads are compared with Choi [6] numerical results.

According to Pierson and Vaziri [20], impactor considered a steel isotropic sphere ($E = 200\ GPa$, $\upsilon = 0.3$) with a radius of 12.7 *mm*, mass of 6.15 *kg* and initial velocity of 1.76 *m/s*. The plate specifications are given in Table 1. It should be noted that the plates examined in these references are quasi-isotropic and are not special orthotropic and contain values A_{16}, A_{26}, D_{16} and D_{26} in their stiffness matrix. However, in many practical cases the laminates have sufficient number of plies to render the coupling vanishingly small (Pierson and Vaziri [20]).

Table 1
Characteristics of the plate used in validating the results (Pierson and Vaziri [20]).

Property and boundary condition		T800H/3900-2 CFRP plate simply supported	
Size: 127×76.2×4.65 *mm*		Layup: $[45/90/-45/0]_{3s}$	
E_{11}	129 *GPa*	G_{12}	3.5 *GPa*
E_{22}	7.5 *GPa*	G_{13}	3.5 *GPa*
υ_{12}	0.33	G_{23}	2.6 *GPa*
Ply thickness	0.194 *mm*	ρ	1540 Kg/m^3

Fig. 10 and Fig. 11 show the comparison of the results of the present models with the references for contact force in CPT and FSDT. As can be seen, the results of these models are in good agreement with the results of Pierson and Vaziri. Because the plate's thickness is out of thin-walled range, the results for FSDT is more accurate than CPT.

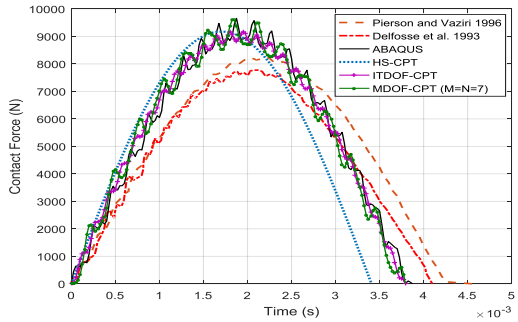

Fig.10
Comparison the results of present models with references and numerical simulation with ABAQUS in CPT (the results of Delfosse adapted from Pierson and Vaziri [20]).

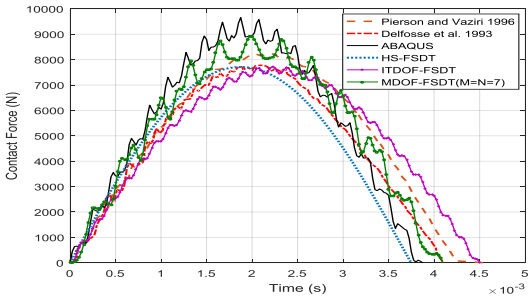

Fig.11
Comparison the results of present models with references and numerical simulation with ABAQUS in FSDT (the results of Delfosse adapted from Pierson and Vaziri [20]).

In order to compare the results including pre-loads with the numerical model of Choi, the impactor considered with a radius of 6.35 *mm*, mass of 1 *kg* and initial velocity of 2.77 *m/s* and the plate specifications are according to Table 2. The initial biaxial load is tension and equal to $3N_{cr}$=2.406e5 *N/m*.

Table 2
Characteristics of the plate used in validating the results (Choi [6]).

Property and boundary condition		Graphite/Epoxy plate simply supported	
Size: 152.4×101.6×2.69 *mm*		Layup: $[0/45/0/-45/0]_{2s}$	
E_{11}	120 *GPa*	G_{12}	5.5 *GPa*
E_{22}	7.9 *GPa*	G_{13}	5.5 *GPa*
υ_{12}	0.3	G_{23}	5.5 *GPa*
Ply thickness	0.135 *mm*	ρ	1580 Kg/m^3

The comparison of the results of the present models with the Choi results for contact force in CPT and FSDT is shown in Fig. 12 and Fig. 13. The figures well illustrate the good performance of the models presented in predicting contact force in presence of pre-loads. The deflection of plate due to impact in CPT and FSDT is shown in Fig. 14 and Fig. 15. This figures also show the good performance of the models presented in predicting the deflection, especially in the MDOF model. In this section, the results are examined for a=b=160 *mm* without changing thickness and h=8 *mm* (h/a=1/20) without changing dimensions and compared with ABAQUS results. The material of the plate used in this section is similar to Pierson and Vaziri (Table 1) and the plate's layup is $[0/90]_{10s}$. The mass of impactor is always 10 times the mass of the plate and the initial velocity of the impactor is selected so that the maximum deflection of the plate is in the linear range (w/h<0.5). Also, the pre-loads applied in two cases $0.25N_{cr}$ and $-0.25N_{cr}$ which the N_{cr} in each method is determined according to the calculated critical buckling load of that method. The critical buckling loads of each method shown in Table 3.

Table 3
Critical buckling load (N/m) for each method.

	ABAQUS	CPT	FSDT
a=b=160 *mm*	1.528e5	1.461e5	1.444e5
h=8 *mm*	1.281e6	1.286e6	1.224e6

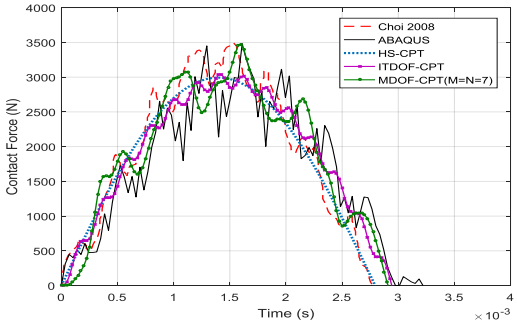

Fig.12
Comparison the results of present models with Choi results and numerical simulation with ABAQUS in CPT.

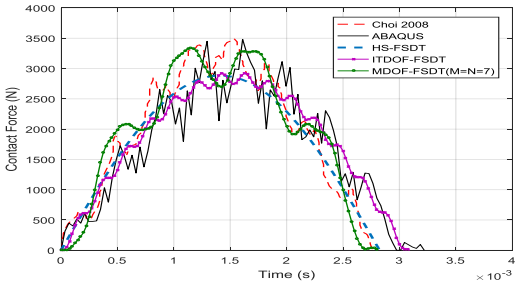

Fig.13
Comparison the results of present models with Choi results and numerical simulation with ABAQUS in FSDT.

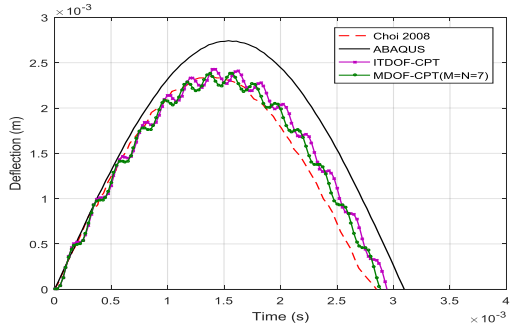

Fig.14
Time history of deflection using current models in CPT and numerical simulation with ABAQUS compared with Choi results.

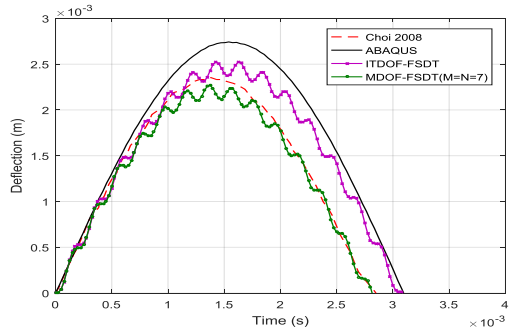

Fig.15
Time history of deflection using current models in FSDT and numerical simulation with ABAQUS compared with Choi results.

Figs. 16 to 19 shows the contact force between the impactor and the plate in the presence of tensile and compressive pre-loads using two theories CPT and FSDT for the dimensional ratio $a/b = 1$. The mass and velocity of the impactor is 1.53 *kg* and 1 *m/s*, respectively. Also, the maximum numerical values of force, final time, and sub-curve level in these four states are given in Table 4. As can be seen, although the plate thickness is 3,875 *mm* and the plate is within the wall-narrow range, the results of the FSDT, especially in the MDOF model, are more favorable than the CPT results. Among the models presented, the results of the MDOF model are much closer to those of Abacus than other models. This is especially true in the maximum force. The results also show that the presence of a pressure precursor reduces the maximum contact force and increases the contact time. At the same time, the area under the force-time curve is almost equal for the two tensile and compressive precursors, and therefore, the force pulse is almost the same.

Table 4
The measured characteristics for $a=b=160$ *mm*.

Theory and pre-load	Model	Final time	Maximum force	Area under the curve
CPT and tension pre-load	ABAQUS	4.620 *ms*	1436.680 *N*	3.056 *N.s*
	HS	4.355 *ms*	1082.724 *N*	3.002 *N.s*
	ITDOF	4.500 *ms*	1105.239 *N*	3.063 *N.s*
	MDOF	4.575 *ms*	1181.591 *N*	3.066 *N.s*
FSDT and tension pre-load	ABAQUS	4.620 *ms*	1436.680 *N*	3.056 *N.s*
	HS	4.430 *ms*	1040.991 *N*	2.936 *N.s*
	ITDOF	4.775 *ms*	1061.965 *N*	3.061 *N.s*
	MDOF	4.800 *ms*	1376.192 *N*	3.112 *N.s*
CPT and compression pre-load	ABAQUS	5.600 *ms*	1181.580 *N*	3.017 *N.s*
	HS	5.524 *ms*	863.106 *N*	3.035 *N.s*
	ITDOF	5.725 *ms*	876.083 *N*	3.062 *N.s*
	MDOF	5.700 *ms*	927.332 *N*	3.075 *N.s*
FSDT and compression pre-load	ABAQUS	5.600 *ms*	1181.580 *N*	3.017 *N.s*
	HS	5.606 *ms*	837.550 *N*	2.989 *N.s*
	ITDOF	5.825 *ms*	849.507 *N*	3.063 *N.s*
	MDOF	5.700 *ms*	1038.373 *N*	3.079 *N.s*

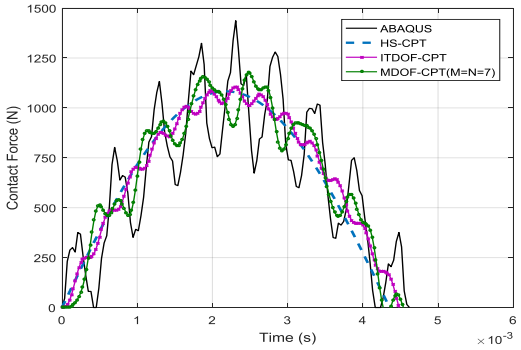

Fig.16
Time history of contact force using current models in CPT and numerical simulation with ABAQUS for $a=b=160$ *mm* in presence of tension pre-load.

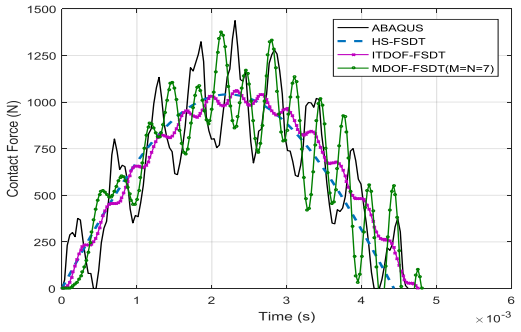

Fig.17
Time history of contact force using current models in FSDT and numerical simulation with ABAQUS for $a=b=160$ *mm* in presence of tension pre-load.

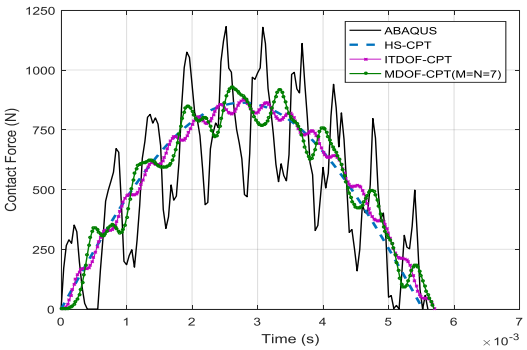

Fig.18
Time history of contact force using current models in CPT and numerical simulation with ABAQUS for $a=b=160$ *mm* in presence of compression pre-load.

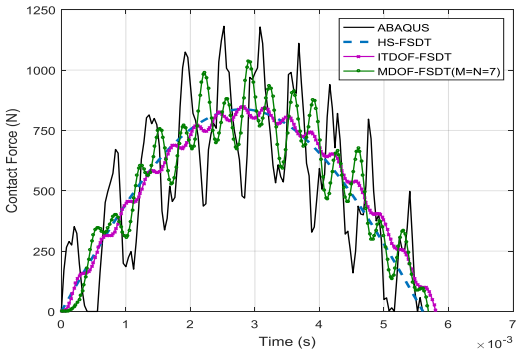

Fig.19
Time history of contact force using current models in FSDT and numerical simulation with ABAQUS for a=b=160 *mm* in presence of compression pre-load.

Figs. 20 to 23 show the contact force between the shock absorber and the plate in the presence of tensile and compressive precursors using two theories CPT and FSDT for a/h = 1/20 ratio. The mass and velocity of the impactor are 3.154 *kg* and 1*m/s*, respectively. Also, the maximum numerical values of force, final time and sub-curve level in these four states are given in Table 5. Because the thickness of the plate in this case is at the boundary of the wall, the results of the MDOF model for CPT are very different from the results obtained from ABAQUS. But this model works very well in FSDT theory. Also, the HS model in FSDT theory has calculated the final time more accurately. In this case, the results of the MDOF model are more in line with the results of ABAQUS than other models, and indicate the superiority of this model over other models.

Table 5
The measured characteristics for h=8 *mm*.

Theory and pre-load	Model	Final time	Maximum force	Area under the curve
CPT and tension pre-load	ABAQUS	2.500 *ms*	5076.350 *N*	6.302 *N.s*
	HS	2.108 *ms*	4141.432 *N*	5.557 *N.s*
	ITDOF	2.450 *ms*	4288.533 *N*	6.335 *N.s*
	MDOF	2.500 *ms*	6199.800 *N*	6.362 *N.s*
FSDT and tension pre-load	ABAQUS	2.500 *ms*	5076.350 *N*	6.302 *N.s*
	HS	2.256 *ms*	3648.148 *N*	5.240 *N.s*
	ITDOF	2.875 *ms*	3785.925 *N*	6.321 *N.s*
	MDOF	2.500 *ms*	4639.305 *N*	6.383 *N.s*
CPT and compression pre-load	ABAQUS	3.060 *ms*	4367.32 *N*	6.275 *N.s*
	HS	2.674 *ms*	3405.016 *N*	5.796 *N.s*
	ITDOF	3 *ms*	3515.122 *N*	6.333 *N.s*
	MDOF	3.175 *ms*	5464.689 *N*	6.440 *N.s*
FSDT and compression pre-load	ABAQUS	3.060 *ms*	4367.32 *N*	6.275 *N.s*
	HS	2.839 *ms*	3077.144 *N*	5.561 *N.s*
	ITDOF	3.300 *ms*	3135.462 *N*	6.308 *N.s*
	MDOF	3.100 *ms*	3798.343 *N*	6.381 *N.s*

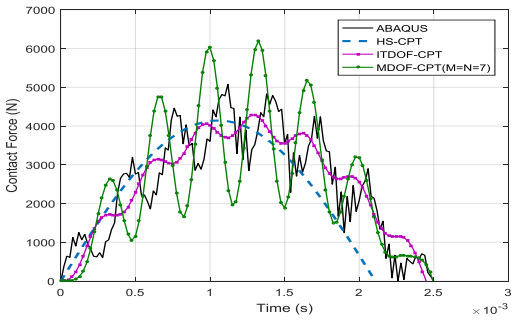

Fig.20
Time history of contact force using current models in CPT and numerical simulation with ABAQUS for h=8 *mm* in presence of tension pre-load.

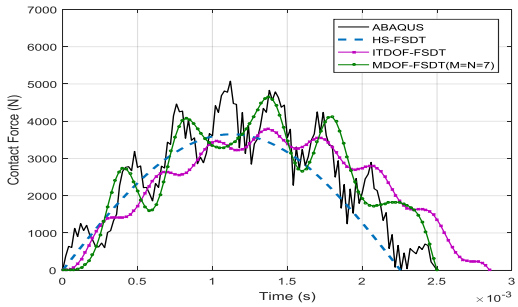

Fig.21
Time history of contact force using current models in FSDT and numerical simulation with ABAQUS for h=8 *mm* in presence of tension pre-load.

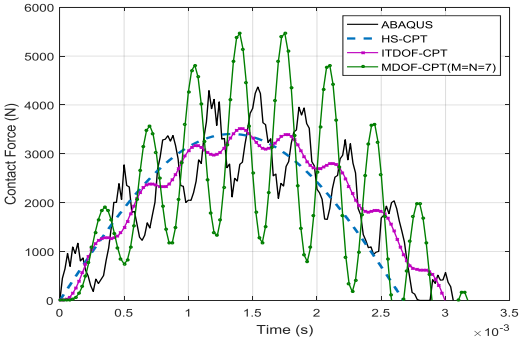

Fig.22
Time history of contact force using current models in CPT and numerical simulation with ABAQUS for h=8 *mm* in presence of compression pre-load.

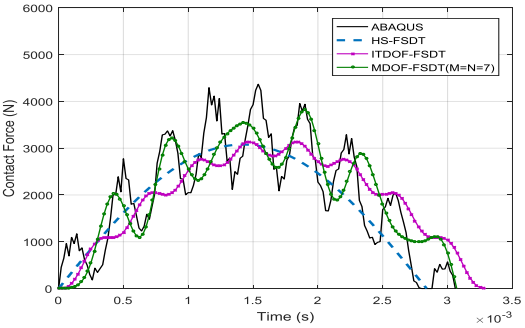

Fig.23
Time history of contact force using current models in FSDT and numerical simulation with ABAQUS for h=8 *mm* in presence of compression pre-load.

In this section, the effect of pre-load on the plate response and the effects of impactor mass at constant velocity and impactor velocity at constant mass are investigated. The FSDT-ITDOF model has been used to evaluate the results. Impactor mass and velocity are considered to be 1.53 *kg* and 1 *m/s*, respectively, a=b=160 *mm* and other specifications are similar to the previous section. The effect of the presence of pre-load on the plate response is shown in Fig. 24. As can be seen, the compressive pre-load decreases the maximum contact force and increases the contact time, while the tensile pre-load increases the maximum contact force and decreases the contact time. Also, the effect of compressive pre-load is greater than tensile pre-load. By applying a compressive pre-load of -0.5 N_{cr} , the maximum contact force is decreased by about 28.57% and the contact time is increased by about 27.14%, while by applying a tensile pre-load of 0.5 N_{cr} , the maximum contact force is increased by about 14.78% and the contact time is decreased by about 13.73%.

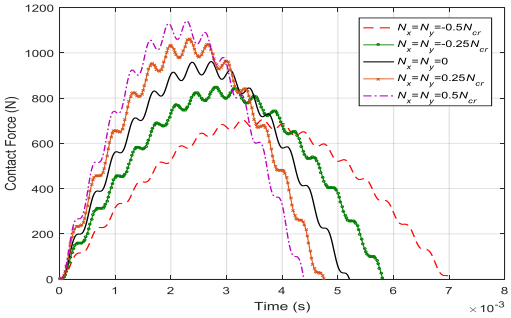

Fig.24
Effect of pre-load on the contact force history.

The effect of the impactor mass on the plate response at $V_0 = 1$ *m/s* is shown in Fig. 25. Increasing the impactor mass increases both the maximum contact force and the contact time. By increasing the impactor mass from 1 to 2 *kg*, the maximum contact force is increased by about 27% and the contact time is also increased by about 28%.

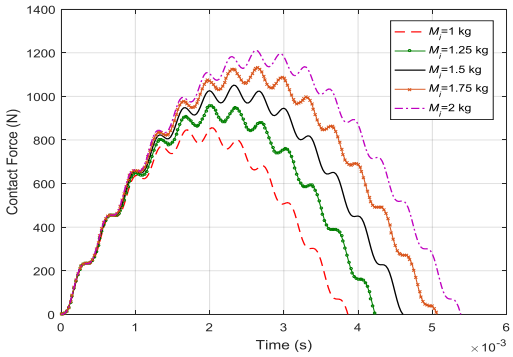

Fig.25
Effect of the impactor mass on the contact force history.

The effect of impactor velocity on the plate response for impactor mass of $M_i = 1.53$ *kg* is shown in Fig. 26. This figure shows that changes in the impactor velocity have no effects on the contact time. However, increasing the impactor velocity increases the maximum contact force. By increasing the impactor velocity from 0.5 to 1.5 *m/s*, the maximum contact force is increased by about 67.3%.

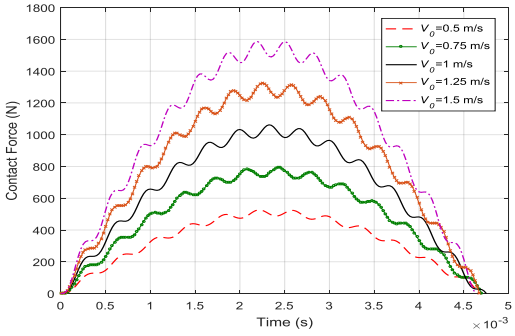

Fig.26
Effect of impactor velocity on the contact force history.

6 CONCLUSION

In this paper, three models for predicting low-velocity impact response on composite plates were presented in the presence of pre-loads. These models are suitable for quasi-static impact. The validation of the results of these models was done using the analytical, experimental and numerical results of the articles available in the references. Also, the results of these models for a special orthotropic plate were compared with the results obtained from ABAQUS software in two modes: $a/b = 1$ dimensional ratio and thickness at wall-to-wall boundary ($a/b = 1.20$). The models presented in this article are simple and have high computational speed. Among the models offered, the MDOF is more accurate than other models, despite its high computational speed.

REFERENCES

[1] Abrate S., 2001, Modeling of impacts on composite structures, *Composite Structures* **51**: 129-138.
[2] Ansari M.M., Chakrabarti A., Iqbal M.A., 2016, Effects of impactor and other geometric parameters on impact behavior of FRP laminated composite plate, *AMSE Journal Series: Modelling A* **89**(1): 25-44.
[3] Apetre N.A., Sankar B.V., Ambur D.R., 2006, Low-velocity impact response of sandwich beams with functionally graded core, *Journal of Solids and Structures* **43**: 2479-2496.
[4] Aslan Z., Karakuzu R., Okutan B., 2003, The response of laminated composite plates under low-velocity impact loading, *Composite Structures* **59**(1): 119-127.

[5] Choi I.H., Lim C.H., 2004, Low-velocity impact analysis of composite laminates using linearized contact law, *Composite Structures* **66**(1-4): 125-132.
[6] Choi I.H., 2008, Low-velocity impact analysis of composite laminates under initial in-plane load, *Composite Structures* **86**: 251-257.
[7] Christoforou A.P., Elsharkawy A.A., Guedouar L.H., 2001, An inverse solution for low-velocity impact in composite plates, *Computers & Structures* **79**: 2607-2619.
[8] Dobyns A.L., 1981, Analysis of simply-supported orthotropic plates subject to static and dynamic loads, *AIAA Journal* **19**(5): 642-650.
[9] Feli S., Karami L., Jafari S.S., 2019, Analytical modeling of low-velocity impact on carbon nanotube-reinforced composite (CNTRC) plates, *Mechanics of Advanced Materials and Structures* **26**(5): 394-406.
[10] Her S.C., Liang Y.C., 2004, The finite element analysis of composite laminates and shell structures subjected to low-velocity impact, *Composite Structures* **66**(1-4): 277-285.
[11] Huo X., Liu H., Luo Q., Sun G., Li Q., 2020, On low-velocity impact response of foam-core sandwich panels, *International Journal of Mechanical Sciences* **181**: 105681.
[12] Karakuzu R., Erbil E., Aktas M., 2010, Impact characterization of glass/epoxy composite plates: An experimental and numerical study, *Composites Part B: Engineering* **41**(5): 388-395.
[13] Khalili S.M., Malekzadeh K., Veysi Gorgabad A., 2013, Low-velocity transverse impact response of functionally graded plates with temperature dependent properties, *Composite Structures* **96**: 64-74.
[14] Khalili S.M., Mittal R.K., Mohammad Panah N., 2007, Analysis of fiber reinforced composite plates subjected to transverse impact in the presence of initial stresses, *Composite Structures* **77**(2): 263-268.
[15] Khalili S.M.R., Soroush M., Davar A., Rahmani O., 2011, Finite element modeling of low-velocity impact on laminated composite plates and cylindrical shells*, Composite Structures* **93**(5): 1363-1375.
[16] Moh J.S., Hwu C., 1997, Optimization for buckling of composite sandwich plates, *AIAA Journal* **35**: 863-868.
[17] Olsson R., 2000, Mass criterion for wave-controlled impact response of composite plates, *Composites Part A* **31**: 879-887.
[18] Patil S., Reddy D.M., Study of oblique low-velocity impact on composite plate, *Materials Today: Proceedings*.
[19] Payeganeh G.H., Ashenai Ghasemi F., Malekzadeh K., 2010, Dynamic response of fiber–metal laminates (FMLs) subjected to low-velocity impact, *Thin-Walled Structures* **48**(1): 62-70.
[20] Pierson M.O., Vaziri R., 1996, Analytical solution for low-velocity impact response of composite plates, *AIAA Journal* **34**(8): 1633-1640.
[21] Setoodeh A., Malekzadeh P., Nikbin K., 2009, Low-velocity impact analysis of laminated composite plates using a 3D elasticity based layerwise FEM, *Materials & Design* **30**(9): 3795-3801.
[22] Shivakumar K.N., Elber W., Lllg W., 1985, Prediction of impact force and duration due to low-velocity impact on circular composite laminates, *Applied Mechanics* **52**: 674-680.
[23] Soedel W., 2004, *Vibration of Shells and Plates*, Marcel Dekker INC, New York.
[24] Swanson S.R., 1992, Limits of quasi-static solutions in impact of composite structures, *Composites Part B: Engineering* **2**(4): 261-267.
[25] Ugural A.C., 2010, *Stresses in Beams, Plates and Shells*, CRC Press, Texas.
[26] Vinson J.R., Sierakowski R.L., 2002,*The Behavior of Structures Composed of Composite Materials*, Kluwer, Dordrecht.
[27] Whitney J. M., Pagano N.J., 1970, Shear deformation in heterogeneous anisotropic plates, *Applied Mechanics* **37**: 1031-1036.
[28] Whitney J.M., 1987, *Structural Analysis of Laminated Anisotropic Plates*, Technomic, Ohio.
[29] Zouggar K., Boukhoulda F.B., Haddag B., Nouari M., 2016, Numerical and experimental investigations of S-Glass/Polyester composite laminate plate under low energy impact, *Composites Part B: Engineering* **89**: 169-186.